Hybrid optimization of driving frequency for crack signature enhancement in nonlinear ultrasonic nondestructive testing

Volodymyr Gatsa, Nesrine Houhat, Sébastien Ménigot

Hybrid optimization of driving frequency for crack signature enhancement in nonlinear ultrasonic nondestructive testing

Volodymyr Gatsa[a,b], Nesrine Houhat[c], Sébastien Ménigot[a,b]

[a] *ESEO, GSII, Angers, France*
[b] *Laboratoire d'Acoustique de l'Université du Mans (LAUM), UMR 6613, Institut d'Acoustique - Graduate School (IA-GS), CNRS, Le Mans Université, Le Mans, France*
[c] *Research Center in Industrial Technologies CRTI, P. O. Box 64, Chéraga 16014, Algiers, Algeria*

Abstract

Nonlinear ultrasonic nondestructive testing methods have largely improved early crack detection in solid materials. However, the nonlinear signature of the crack can be difficult to measure. In this paper, to overcome this drawback, we present a parametric optimization to automatically find the best driving frequency which maximizes the nonlinear signature. The optimization process is carried out in two steps to maximize a cost function corresponding to the nonlinear-linear ratio (NLR). From the signal received, NLR assesses the energy of the second harmonic over the energy of the fundamental component. This optimization is achieved by the hybridization of two algorithms: the genetic algorithm and the Nelder-Mead algorithm. The method is applied experimentally on a duraluminium sample including a crack. The optimal frequency is obtained after less than 14 iterations only. Moreover, the gain of the nonlinear-linear ratio reaches up to 12 dB in comparison with that obtained by the usual frequency setting.

Keywords: Driving frequency, Nondestructive evaluation, Hybrid optimization, Nonlinearity, Crack signature enhancement

No conflicts of interest.

Highlights

- The driving frequency is automatically set to enhance nonlinear signatures of cracks.
- The optimal driving frequency is found using hybrid optimization.
- The optimization is applied experimentally on a duraluminium sample.
- The gain of the nonlinear-linear ratio reaches up to 12 dB.

1. Introduction

In industrial applications, ultrasonic nondestructive testing (NDT) is widely used to assess the integrity of materials by detecting defects such as fatigue, cracks, fractures, delamination, corrosion, thermal aging, and hardening [1]. The conventional ultrasonic NDT principle is based on sending an ultrasonic wave packet at a driving frequency f_0 and then receiving the propagated waves at the same frequency f_0. On the one hand, linear NDT methods can detect the defects by means of their impedance mismatch with the surrounding medium. On the other hand, they can extract the local mechanical properties. Nevertheless, conventional techniques are unable to detect microstructural changes, such as internal microcracks and microvoids. These changes may limit the applicability and resolution of conventional techniques, especially in complex and heterogeneous materials [2].

To overcome this limitation, NDT based on nonlinear acoustic phenomena have emerged. These techniques began to gain popularity over the last decades due to their practical advantage in detecting micro-damage where conventional linear techniques remain blind [3, 4]. They are based on the assumed, much larger, nonlinear response of cracks, imperfect interfaces, or more generally, internal solid contacts, compared to undamaged homogeneous parts of the material. Thus, local nonlinear wave interaction effects occur preferentially at defects. Monitoring their signatures provides a selective means of characterization of a sample. Moreover, the possible nonlinear interaction effects are various, which leads to various methods being proposed. Among these methods, we can cite the study of nonlinear amplitude dependence on measured parameters (attenuation, velocity, *etc.*) [5] and the amplitude-dependent shift of resonance frequencies (Nonlinear Resonance Ultrasound Spectroscopy or NRUS) [6]. However, these techniques may require several measurements to provide a diagnosis of the material, which can be considered as a drawback. The harmonic generation technique overcomes this problem by sending an ultrasonic wave at a driving frequency f_0 and by receiving the nonlinear response generated by the crack at the harmonic frequencies $2f_0$, $3f_0$ [7]. This principle was extended to the cases of sub and ultra harmonic generation [8]. In order to overcome the nonlinearity of the measurement system (*e.g.* nonlinearity of electronic devices), other techniques are used such as Nonlinear Wave Modulation Spectroscopy (NWMS) [9]. With this method, a sample is excited simultaneously by two waves; a low and a high frequency wave. By the presence of nonlinear phenomena (*i.e.* a crack in a sample), the high frequency will be modulated by a low frequency wave. This wave intermodulation thus generates sideband components located at the sum and difference of the two driven frequencies [10].

Furthermore, signal post-processing tools are important to distinguish nonlinear effects coming from the crack in the sample. Usually, the nonlinear components are extracted with digital filters. Some other techniques are based on several discrete encoding signals with multiple transmissions such as the pulse inversion method [11] and the scaling subtraction method [12]. Others are based on nonlinear signal processing models, such as the Hammerstein model [13] and

Volterra model [14].

Nevertheless, due to experimental particularities, inherent to the sample and instrumentation (*e.g.* electronics and transducers), signal post-processing techniques are not sufficient and nonlinear effects can be hidden and cannot then be discriminated. Firstly, in the ultrasound domain, the transfer function of the transducer is quite limited due to its bandwidth [15]. Thus, to measure harmonic components, a transducer with a large bandwidth should be used. However, a simpler solution can be used by adding another transducer in reception with a central frequency equal to double the driving frequency. Secondly, nonlinear signatures are highly dependent on the driving wave. For example, with a low drive amplitude, the nonlinear effect can be annihilated. In contrast, a high drive amplitude will lead to an acoustic saturation and unjustified results [16]. Another example is the local defect resonance [17] which facilitates the defect recognition. But it remains hard to control [18]. Therefore, it is clear that the transmitted signal has an influence on the quality of the received signal [19].

Based on this information, a signal pre-processing step should be necessary. Usually, an empirical choice of driving signal parameters is carried out in material inspection, such as the driving frequency [20] or the drive amplitude [21]. For example, the choice of driving frequency can be based only on the bandwidth of the reception transducer to measure the second harmonic, for example the driving frequency is set to 2/3 of the center frequency of the receiving transducer in medical imaging [22]. To find the best driving signal, some authors have suggested continuously sweeping the driving frequency by a chirp [23]. However, the problem remains complex, since it is necessary to define the chirp coefficients, by taking into account information about the medium and the instrumentation [24]. This drawback has been overcome by automatically selecting the best driving parameters without *a priori* information of the system. Lately, the optimal frequency command principle has been implemented for medical ultrasound imaging within driving frequency optimization [25]. It has been expanded to a waveform optimization of the driving signal [26, 27]. Moreover, an optimal frequency selection has been applied in NDT for metal inspection using the vibro-acoustic modulation (VAM) method [28]. However, the optimal frequency command has not already been applied on solid materials, if it is not possible to apply a pump frequency (the low-frequency excitation in VAM method). This paper is an extension of the optimal frequency command application to solid materials inspection. Its main goal is to improve the nonlinear NDT performance to crack detection by the enhancement of the nonlinear crack signature. Since the optimal command can be used for all nonlinear NDT methods, we are focusing this study on the second harmonic enhancement technique [29, 30]. A feasibility study for optimizing the driving frequency has already been presented in simulation [31]. The present work is dedicated to the experimental validation of driving frequency optimization. The optimal command is applied for both cracked and healthy samples. In order to quantify the nonlinear crack signature, a cost function called Nonlinear Linear Ratio NLR made from [32] has been considered. Moreover, to be more robust than in previous studies and to find the global maximum, the optimization of NLR as a

function of the driving frequency has been implemented by a hybridization of two optimization algorithms: the genetic and Nelder-Mead algorithms.

The paper starts with a description of the optimal frequency command in NDT. Then, the experimental validation takes place. The results obtained with the optimal frequency command are compared with those obtained with the empirical frequency sweep. The paper ends with a discussion and a conclusion.

2. Optimal Frequency Command for nonlinear NDT

Optimal command is based on finding the optimal driving frequency f_{opt} by adding a closed loop optimization. It can enhance the nonlinear signature of the crack. The optimal frequency is classically identified by the following expression:

$$f_{opt} = \arg\max_{f_k} \left[NLR(f_k) \right], \tag{1}$$

where f_{opt} is the optimal driving frequency which provides the best value of the cost function NLR. Note that we define NLR in the subsection 2.2 from the generated second harmonic by taking into account the limited transducer bandwidth in the reception. The iterative approach is implemented to solve the Equation 1, as shown in the block diagram in Fig. 1.

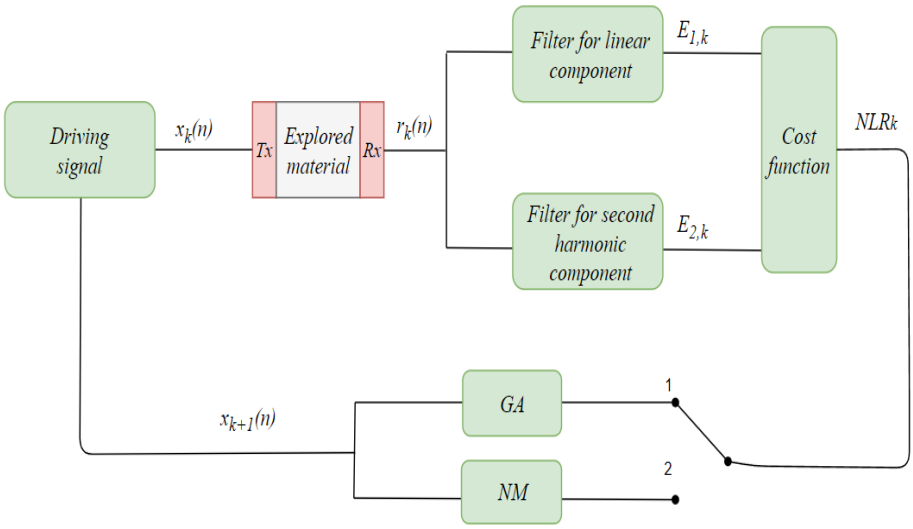

Figure 1: Block diagram of the closed loop optimization method for optimal frequency assessment. NM: Nelder–Mead algorithm. GA: genetic algorithm.

Following the iterative optimization, a driving signal $x_k(n)$ is transmitted to the medium at the driving frequency f_k, for the iteration k (where n is the discrete time). The received signal $r_k(n)$ is recorded. It is then filtered by adjusted digital bandpass filters to extract the desired nonlinear information. The cost function NLR_k is thus calculated. Finally, feedback is added to maximize

NLR by selecting a new driving signal $x_{k+1}(n)$ at a new driving frequency f_{k+1} for the next iteration $k+1$. These steps are then repeated until the optimal frequency f_{opt} is reached.

Moreover, in order to find the global maximum, the optimization process combines two optimization algorithms. In a first step (switch position 1 in Fig. 1), a genetic algorithm (GA) is used to find the region of the global maximum. Later, after a fixed number of iterations, the switch is moved to position 2 in Fig. 1. A Nelder-Mead algorithm (NM algorithm) is then initialized with the last iteration of GA. Note that the purpose of this second step is to refine the results of the GA [33].

2.1. Driving Signal and Driving Frequency

At iteration k, a driving signal x_k is transmitted with a fixed driving frequency f_k. The waveform is a Gaussian modulated sinusoidal pulse with a relative fractional bandwidth of 40% as follows:

$$x_k(n) = A \cdot \exp\left(-\frac{\left(\frac{n}{F_s} - \frac{L}{2 \cdot F_s}\right)^2}{(\frac{L}{2 \cdot F_s})^2}\right) \cdot \sin\left(2\pi \cdot f_k \cdot \frac{n}{F_s}\right) \tag{2}$$

where F_s is the sampling frequency, n the discrete time, A the drive voltage amplitude, f_k the driving frequency at iteration k, L the duration of the driving signal and $\frac{L}{2 \cdot F_s}$ the central time of the Gaussian pulse. Note that the relative fractional bandwidth is limited to 40%, based on our experience, in order to generate harmonics, while limiting the duration of the driving signal L.

Moreover, in the present method, the driving signal is generated with a constant drive power. This constraint guarantees constant drive power at various driving frequencies. The constant drive power is made by adjusting the magnitude of the driving signal amplitude for each driving frequency as follows:

$$A = A_{ref} \cdot \frac{P_{ref}}{P_{f_k}}. \tag{3}$$

where A_{ref} is the reference drive amplitude, P_{ref} the reference drive power of a Gaussian pulse (Equation 2) at frequency f_{ref}, P_{f_k} the drive power at driving frequency f_k computed by:

$$P_{f_k} = \frac{1}{L} \sum_{n}^{L} x_k^2(n). \tag{4}$$

For instance, this reference driving frequency f_{ref} could be the central frequency of the transmission transducer.

2.2. Cost Function NLR

The received signal $r_k(n)$ is measured. Filtering is carried out by the two adjusted Butterworth band-pass filters, in order to separate fundamental and

second harmonic components. Thus, the first and second filters are respectively centered at f_c and $2f_c$. The central frequencies f_c of both filters are adjusted by taking into account the slight shift of the observed central frequency, mainly due to the instrumentation bandwidth. Furthermore, the bandwidth of each filter is $m \cdot f_c/10$ for -3 dB with $m = \{1, 2\}$ to extract the fundamental and second harmonic components respectively.

The received energies of fundamental and second harmonic components are, thus, calculated in the time domain as:

$$E_m = \sum_{n=0}^{N-1} \left(r_k(n) * h_m(n) \right)^2 , \tag{5}$$

where $r_k(n)$ is the discrete received signal, N the number of received samples, $h_m(n)$ the infinite impulse response of the Butterworth bandpass filter and $*$ the convolution symbol.

Finally, in our case, the cost function is the ratio of the second harmonic energy over the fundamental harmonic energy. We call it Nonlinear-Linear Ratio (NLR) and it is defined as:

$$NLR = 10 \cdot \log_{10} \left(\frac{E_2}{E_1} \right) . \tag{6}$$

The maximization of this cost function means that the second harmonic energy is increased while the fundamental energy is decreased.

2.3. Hybrid Optimization

In the present study, the hybrid approach aims to increase the optimization robustness with more precision [34], by combining two algorithms : a global optimization with the genetic algorithm (GA) and a local optimization with the Nelder Mead algorithm (NMA). This hybridization must guarantee the convergence to the global maximum with precision, regardless of the convergence speed. If the cost function NLR is convex, hybridization using GA is useless and the NMA is sufficient. However, in practise, it can be difficult to know if the cost function NLR is convex.

In the first step of the hybrid algorithm, the global maximum of NLR is found by implementing GA, which is a type of metaheuristic algorithm. It is run by the principle of natural selection by relying on biologically inspired operators such as mutation, crossover and selection [35, 36]:

1. for the first generation $k = 1$, the initial population of 12 frequencies is selected randomly from a uniform distribution from f_{min} to f_{max}. The choice of these values is directly related to the bandwidth of the transducer and the amplifier. It restricts the frequency interval to the system bandwidth in order to avoid unnecessary measurements and processing;
2. then, for the same generation, the GA evaluates the cost function NLR for the 12 frequencies of the population. The 12 cost function values are

sorted in descending order with the corresponding driving frequencies. GA returns the best frequency value which maximizes the cost function NLR. Note that the frequency at the first generation is thus the best solution among the 12 frequencies of the initial population;

3. for next generations (*i.e.* $k+1$), the population is built from the previous generation k. The first six best driving frequencies (*i.e.* 50% of the population) are kept and become parents. The crossover operator enables the creation of new driving frequencies called offspring. Therefore, new frequencies are generated by mating between frequencies of each generation. This mating is described with the following equation:

$$f_{child} = f_m \pm \beta[f_m - f_d], \tag{7}$$

where f_{child} is the new proposed frequency, f_m and f_d are respectively the mother and father frequencies, β a random coefficient between 0 and 1. Then, the mutation is applied at the rate of 40%. Note that these three settings have been proposed in [36] and confirmed by our experience.

4. Finally, if the stopping criterion is not reached, the next iteration starts again from step 2. Based on our experience, after 8 iterations, the GA was stopped to limit the experiment's duration. Throughout these eight generations, the driving frequency converges to the region of the global maximum. Note that the number of generations is limited to reduce the number of measurements.

It is appropriate to emphasize that the exploited GA is used to remedy the inability of the NMA to find the global maximum [36], by initializing it in the right frequency range. If the cost function NLR is not convex, the NMA can be stuck on local maxima. Fortunately, the region of the global maximum can be found using metaheuristics (GA). Therefore, the two algorithms are complementary. On the one hand, the GA does not need any special initialization. On the other hand, the NMA is more efficient at converging to the accurate solution in a few iterations. But it needs to be correctly initialized.

Thereafter, the Nelder–Mead method [37] is initialized with the best driving frequency f_{init} obtained by GA. It maximizes the cost function NLR with precision and without any derivative information (explicit or implicit). It is based on the concept of simplex, which generalizes the triangle. The principle of the algorithm is to frame the maximum. At each iteration, the cost function is evaluated for each vertex of the simplex. Then, the algorithm computes the centroid of the simplex and the reflection point of the centroid. Then, the NMA expands, contracts and shrinks the simplex to get closer to the function maximum. Note that a flow chart of the NMA has been shown in [37].

3. Experimental setup

The experimental setup follows the steps described in Fig. 2 as explained in section 2.

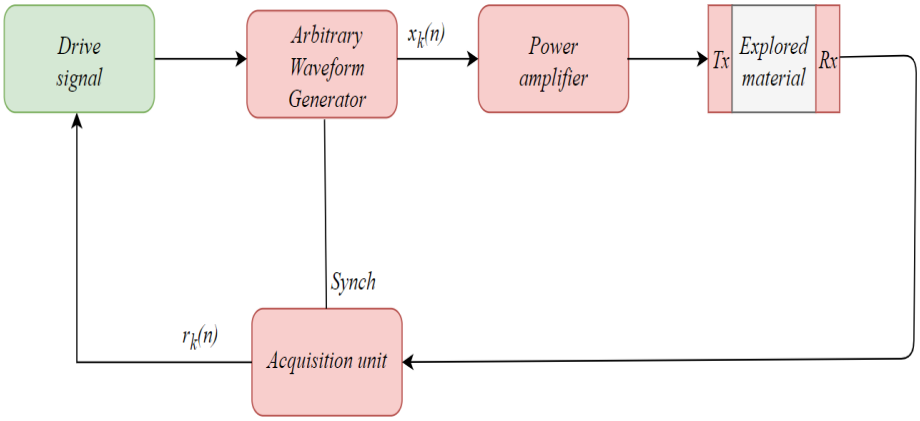

Figure 2: Functional diagram of the experiment. $x_k(n)$ is discrete driving signal; $r_k(n)$ discrete received signal

The driving signal $x_k(n)$ at the driving frequency f_k is generated digitally by Matlab (Matlab R2018b, The Mathworks, Inc., Natick, Massachusetts, USA). It is then transmitted to a computer-controlled arbitrary waveform generator (Agilent 33225A, Santa Clara, CA, USA). Next, the driving signal $x_k(n)$ is adjusted taking into account the reference drive amplitude A_{ref} of 3 V and the reference frequency f_{ref} of 1 MHz. It is then amplified by a 200 W power amplifier (Model AAP-200-1-10, Adece, Veigné, France) with a gain of 50 dB. Note that the power amplifier is linear in the bandwidth between 1 and 10 MHz. A transmit angle beam transducer AT014 (Valpey Fisher, Albuquerque, NM, USA) with the diameter of 0.5 inches (12.5 mm) transmits the amplified signal to the inspected medium (as Tx in Fig. 3). Impedance matching is provided by water-soluble ultrasound transmission gel.

The sample studied is a simple duraluminium bloc with a dimension of $8.9 \times 9.3 \times 1.2$ cm (Fig. 3). The material has a 6 cm notch extended by a crack obtained after a fatigue test. The crack width varies by a few tenths of a micrometer to a few millimeters. The transducers are placed on both sides of the crack.

The output ultrasonic signal is measured with a transducer (AT022, Valpey Fisher, Albuquerque, NM, USA) centered at 2.25 MHz. This transducer with a 0.25 inch diameter is placed at a distance of 5 cm from the transmit transducer (as Rx in Fig. 3), according to a template. Moreover, it is on a wedge at an angle of 45° to the sample surface to directly receive echoes coming from the crack. The output signal is acquired by a digital converter (Pico 5000, PicoTech, St Neots, UK) and triggered by the arbitrary waveform generator. The acquisition is made with the memory depth N of 8192 points at a sampling rate F_s of 62.5 MHz. Moreover, in order to improve the signal-to-noise ratio, an average of 64 successive acquisitions is carried out. This output averaged signal is finally recorded as $r_k(n)$.

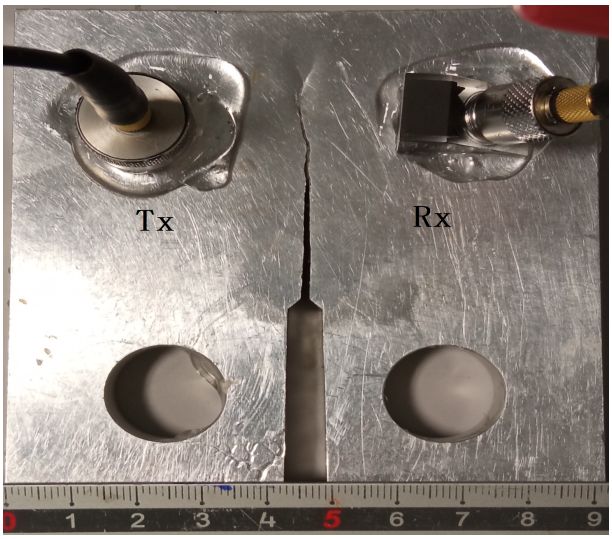

Figure 3: Cracked sample. Transmitter on the left, receptor on the right.

Before extracting harmonic components to compute the cost function NLR_k, prefiltering is done. It must ensure that the linear mode of the power amplifier is maintained as in its specification between 1 and 10 MHz. Thus $r_k(n)$ is filtered between 1 and 10 MHz (the bandwidth of the power amplifier) and between 2 and 20 MHz to extract the fundamental and the second harmonic, respectively. Note that if the power amplifier is linear on a higher bandwidth, prefiltering can be removed.

Finally, a single cost function NLR_k is calculated from E_1 and E_2 (equation 6). However, to guarantee better robustness, the final cost function NLR_k is assessed from the median of 10 single cost function measurements. This repetition could be higher to decrease measurement uncertainty.

As a comparison, the material studied can be changed. In this study, an intact material is used. It has similar properties to the cracked sample (except the crack). The transducers are rigorously placed on the intact sample surface, according to the same template used for the crack material.

4. Results

In this section, the results are presented in the following three steps. Firstly, empirical scanning is proposed to assess the cost-function NLR for both intact and cracked materials. Secondly, closed loop optimization by GA is performed to reach the region of the maximum of NLR. Finally, the GA optimization results are refined by the NMA.

4.1. Empirical scanning

Empirical scanning for both intact and cracked materials is presented in Fig. 4. Empirical scanning was done in the frequency range from 0.8 to 2.5 MHz with a step of 50 kHz. This scan range was chosen to ensure good signal reception according to the bandwidth of the transducer in reception. For each frequency, the cost function *NLR* is assessed 20 times. The assessment median is represented by solid lines. The variations between different assessments are represented by bars as are the variations between the 4th and 6th deciles.

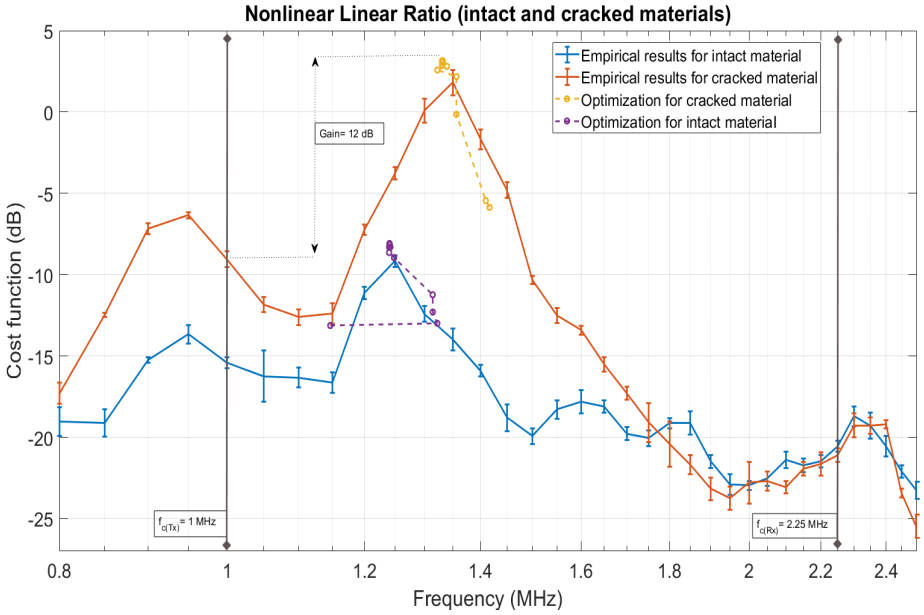

Figure 4: Empirical scan of the cost function *NLR* versus driving frequency (solid line). Automatic optimization by the GA and the NA algorithm (dashed lines). $f_{c(Tx)}$: central frequency of the transmission transducer, $f_{c(Rx)}$: central frequency of the reception transducer.

The global maximum of *NLR* is located at a frequency of 1.35 MHz for the cracked material and reaches 1.81 dB, *i.e.* the second harmonic energy is higher than the fundamental energy. As for comparison, the global maximum of *NLR* is located at 1.25 MHz for the intact material and remains low (-9.16 dB), *i.e.* the second harmonic energy is very low compared to the fundamental energy.

Another observation is that *NLR* shows several local maxima and global optimization with the GA is thus required for automatic optimization. However, because of the sweeping, the best frequency is known with a precision of 50 kHz.

Furthermore, *NLR* for the cracked material is globally higher compared to *NLR* for the intact material. Near to the global maximum, there is no overlap between the two curves for cracked and intact materials. For each of the driving frequencies, the variations between the 20 repetitions are small, between 1 and 3 dB. However, this is not the case for higher driving frequency values, as of

1.8 MHz, where NLR is low whatever the material. This means that the second harmonic energy is very low compared to the fundamental energy. It is important to notice that nonlinearities could come from sources other than a crack, such as, for example, transducer contact or an electronic device. However, in this case, the same behaviour in cracked and intact material would be expected. This increase can therefore be explained by the presence of the crack.

Finally, the gain can reach 12 dB in comparison to the usual case where the driving frequency is at the central frequency of the transmission transducer ($f_{c(Tx)} = 1$ MHz) defined as the usual setting.

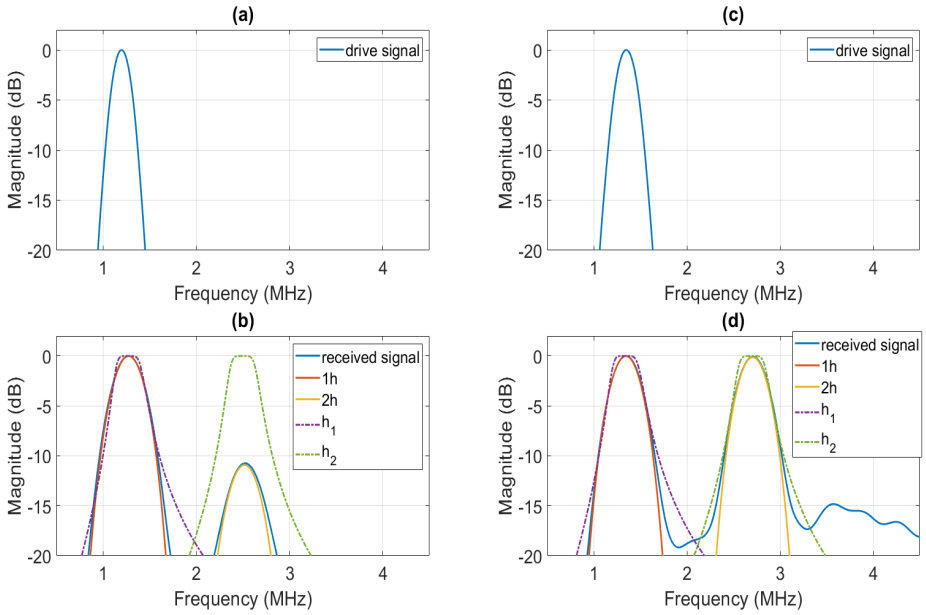

Figure 5: Received signals spectra at the frequencies with the maxima NLR after empirical scanning for the intact material (b) and the cracked material (d) with the corresponding spectra of the driving signals at 1.2 MHz and 1.35 MHz transmitted to intact (a) and cracked (c) materials. h_1, h_2 transfer functions of filters; $1h$, $2h$ filtered received signals at fundamental and second harmonics.

Fig. 5a and Fig. 5c illustrate the spectra of driving signals for which the NLR is maximal in empirical scanning for the intact and the cracked material respectively. Fig. 5b and Fig. 5d represent the spectra of the received signals respectively. Their filtered components at the frequencies of the fundamental (written $1h$) and second (written $2h$) harmonics are also added. In Fig. 5b, the magnitude at the second harmonic is 13 dB lower than the fundamental harmonic. In comparison, for Fig. 5d the magnitude at the second harmonic is on the same level as at the fundamental one. These results are consistent with the same measurements of the cost function calculated from the energies of both components. Consequently, the energy is proportional to the area under the curve. In both Fig. 5b and 5d, the filter transfer functions are represented

as h_m described in the Equation 5.

4.2. Optimization by Algorithms

Hybrid optimization between GA and NMA algorithms is presented in Fig. 6 and Fig. 7 for cracked and intact materials respectively.

Fig. 6a and Fig. 7a show the driving frequency settings through iterations of the GA and the NMA.

The first eight driving frequencies were computed iteratively by GA. The optimal driving frequency reached by the GA is respectively 1.35 MHz and 1.31 MHz for the cracked and intact material. Note that the initial population is included in a frequency range from $f_{min} = 0.9$ MHz to $f_{max} = 2.5$ MHz. As previously explained, the choice of the initial frequency range is directly related to the bandwidth of the transducer and the amplifier. We could have chosen a larger frequency range. But we have restricted the frequency interval to the system bandwidth in order to avoid unnecessary measurements and, consequently, to speed up the algorithm convergence.

Then, the NMA was initialized from the result obtained by GA (f_{init}). The following driving frequencies were computed by the NMA. The NMAs reach the *NLR* convergence and find the optimal driving frequency at $f_{opt,crack} = 1.33$ MHz for the cracked material and at $f_{opt,int} = 1.24$ MHz for the intact material.

In order to check the measurement robustness by correct initialization of NMA, the NMA was repeated 10 times from the GA result. Variation bars were added to show the frequency variation between repetitions of ten NMA optimizations (the median is represented by lines and variations between the 4^{th} and 6^{th} deciles are represented by bars). In the case of cracked material, driving frequency variations, during iterations, did not exceed 7 kHz. However, they reached 30 kHz for intact material because of the low *NLR* levels. Note that no variation bars are shown during GA, because this step aims to find the region of global maximum only (without precision).

Fig. 6b and Fig. 7b show the cost function *NLR* variations through iterations for the driving frequencies shown respectively in Fig. 6a and Fig. 7a.

The GA converged in the region to the global maximum, after 3 generations for the cracked material and 7 iterations for the intact material. The global maxima were at -0.15 dB and at -12.3 dB for cracked and intact material respectively.

During the GA step, each single measurement of *NLR* was repeated 10 times (*i.e.* for each frequency of each generation of the GA) to increase the robustness of the instrumentation. Variations bars were added to show the *NLR* variation between the ten measurements during GA optimization (median is represented by the lines and variations between the 4^{th} and 6^{th} deciles are represented with the bars). *NLR* variations during generations stayed low, less than 0.5 dB.

Then NMA was launched from the last GA result. It converged after 4 iterations and refined the global maximum to reach 3.15 dB for the cracked material and -8 dB for the intact material. Fourteen iterations (8 for GA and 6 for NMA) were sufficient to reach the global maximum with hybrid optimization.

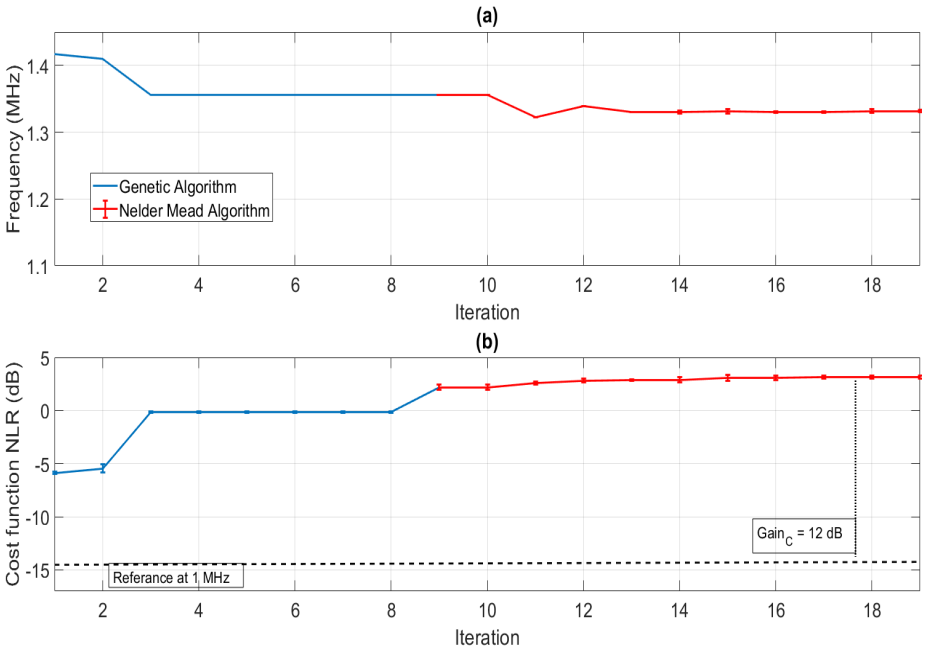

Figure 6: Results of combined hybrid optimization by algorithms (Genetic, Nelder-Mead) for the cracked material. (a) Driving frequency *vs.* iterations. (b) cost function vs. iterations.

Moreover, as explained previously for the frequency settings, the whole optimization process from NMA was also repeated ten times. *NLR* variations during iterations are only 0.5 dB for cracked material and between 0.5 and 3 dB for the intact sample.

These results are in agreement with those obtained by empirical scanning. As an illustration, we have added the optimization for both materials (cracked and intact) in Fig. 4. Indeed, small differences can be noted between empirical scanning and automatic optimization. This can be explained by (i) the variations between repetitions and (ii) the limited knowledge of *NRL* after empirical scanning (only computed for a few frequencies).

Finally, to summarize, the *NLR* maximum was higher for the cracked material. Therefore, the difference between optimal values of the *NLR* for cracked and intact materials was 11.2 dB, *i.e.* a ratio 13 times greater. This optimal performance result should lead to more sensitive and reliable possible crack detection at optimal frequency.

5. Discussion and Conclusions

In the present work, nonlinear crack signature enhancement is performed by adding feedback to an open-loop conventional ultrasound system. The main idea consists of finding the input driving frequency by optimizing the cost func-

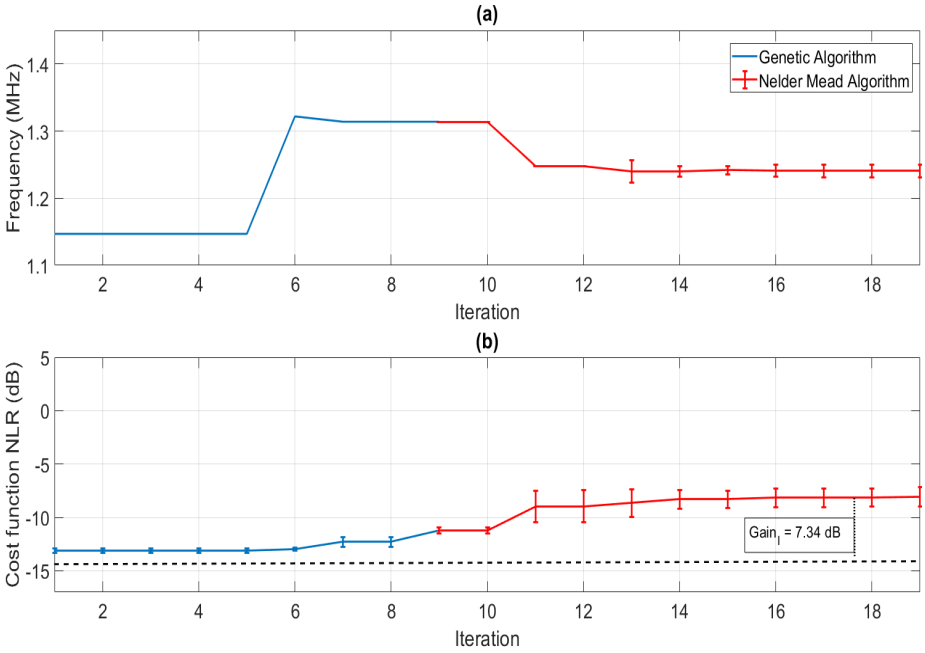

Figure 7: Combined hybrid optimization by algorithms (Genetic, Nelder-Mead) for the intact material. (a) Driving frequency *vs.* iterations. (b) cost function vs. iterations.

tion *NRL*, *i.e.* maximizing the second harmonic energy while minimizing the fundamental energy. The optimal driving frequency has been adjusted automatically by the hybridization of two optimization algorithms by following two steps: (i) select the region of the global maximum, by GA and (ii) refine global maximum result by NMA. Therefore, the method experimentally turns the empirical scanning into optimal scanning to find the optimal frequency in just a few measurements. Unlike empirical sweeping with a given frequency resolution, this optimization focused the measurements as close as possible to the *NLR* maximum.

This optimization allows us to reach a gain of up to 12 dB in comparison with the fixed central frequency of the transmission transducer. The main reason of this increase is a better ability to receive the second harmonic by the reception transducer. This property is taken into account in the cost function *NLR*. Indeed, the latter includes implicit information about medium properties, crack properties and electronic devices. Thus, the optimization process does not require *a priori* information.

Our method deals with media including cracks with nonlinear behavior. Therefore, the electronic devices have to be linear, at least over the studied frequency range. In the opposite case, a constraint could be added from the received signal, like, for example, with complementary filtering.

To conclude, as nonlinear cracks can have a small signature, it is crucial to

achieve optimal settings of the experimental setup. The added closed loop could help to make these adjustments, applied here to the driving frequency. Thus, the optimal frequency command should be useful to improve crack detection. It may lead to a further step of classification between cracked and intact materials.

Acknowledgements

This work was supported by the WISE program in the Pays de la Loire region (Project COSINUS – Optimal command of smart sensors for nonlinear ultrasound).

References

[1] J. Blitz, G. Simpson, Ultrasonic methods of non-destructive testing, Vol. 2, Springer Science & Business Media, 1995.

[2] P. B. Nagy, Fatigue damage assessment by nonlinear ultrasonic materials characterization, Ultrasonics 36 (1-5) (1998) 375–381.

[3] I. Y. Solodov, Ultrasonics of non-linear contacts: propagation, reflection and nde-applications, Ultrasonics 36 (1-5) (1998) 383–390.

[4] I. Solodov, N. Krohn, G. Busse, Nonlinear ultrasonic ndt for early defect recognition and imaging, in: European Conf. on NDT (ECNDT), Moscow, Citeseer, 2010.

[5] D. Yanwu, T. Jie, S. Yongchen, Relations between the acoustic nonlinearity parameter and sound speed and tissue composition, in: IEEE 1987 Ultrasonics Symposium, IEEE, 1987, pp. 931–934.

[6] K. Van Den Abeele, F. Windels, Characterization and imaging of microdamage using nonlinear resonance ultrasound spectroscopy (nrus): An analytical model, in: Universality of Nonclassical Nonlinearity, Springer, 2006, pp. 369–388.

[7] M. Breazeale, D. Thompson, Finite-amplitude ultrasonic waves in aluminum, Applied Physics Letters 3 (5) (1963) 77–78.

[8] I. Solodov, J. Wackerl, K. Pfleiderer, G. Busse, Nonlinear self-modulation and subharmonic acoustic spectroscopyfor damage detection and location, Applied physics letters 84 (26) (2004) 5386–5388.

[9] K.-A. Van Den Abeele, P. A. Johnson, A. Sutin, Nonlinear elastic wave spectroscopy (news) techniques to discern material damage, part i: nonlinear wave modulation spectroscopy (nwms), Journal of Research in Nondestructive Evaluation 12 (1) (2000) 17–30.

[10] A. Sutin, P. Johnson, Nonlinear elastic wave nde ii. nonlinear wave modulation spectroscopy and nonlinear time reversed acoustics, in: AIP Conference Proceedings, Vol. 760, American Institute of Physics, 2005, pp. 385–392.

[11] T. Goursolle, S. Callé, S. Dos Santos, O. Bou Matar, A two-dimensional pseudospectral model for time reversal and nonlinear elastic wave spectroscopy, The Journal of the Acoustical Society of America 122 (6) (2007) 3220–3229.

[12] M. Scalerandi, A. Gliozzi, C. Bruno, D. Masera, P. Bocca, A scaling method to enhance detection of a nonlinear elastic response, Applied Physics Letters 92 (10) (2008) 101912.

[13] F. Sbeity, S. Ménigot, J. Charara, J.-M. Girault, Contrast improvement in sub-and ultraharmonic ultrasound contrast imaging by combining several hammerstein models, International journal of biomedical imaging 2013 (2013).

[14] P. Phukpattaranont, E. S. Ebbini, Post-beamforming second-order volterra filter for pulse-echo ultrasonic imaging, IEEE transactions on ultrasonics, ferroelectrics, and frequency control 50 (8) (2003) 987–1001.

[15] M. Pollakowski, H. Ermert, Chirp signal matching and signal power optimization in pulse-echo mode ultrasonic nondestructive testing, IEEE transactions on ultrasonics, ferroelectrics, and frequency control 41 (5) (1994) 655–659.

[16] F. A. Duck, Nonlinear acoustics in diagnostic ultrasound, Ultrasound in medicine & biology 28 (1) (2002) 1–18.

[17] J. Segers, M. Kersemans, E. Verboven, S. Hedayatrasa, J. Calderon, W. V. Paepegem, Investigation to local defect resonance for non-destructive testing of composites, in: Multidisciplinary Digital Publishing Institute Proceedings, Vol. 2, 2018, p. 406.

[18] V. V. Kazakov, A. Sutin, P. A. Johnson, Sensitive imaging of an elastic nonlinear wave-scattering source in a solid, Applied Physics Letters 81 (4) (2002) 646–648.

[19] J. Smith, The joint optimization of transmitted signal and receiving filter for data transmission systems, Bell System Technical Journal 44 (10) (1965) 2363–2392.

[20] M. Bramanti, A nondestructive diagnostic method based on swept-frequency ultrasound transmission-reflection measurements, IEEE transactions on instrumentation and measurement 41 (4) (1992) 490–494.

[21] D. Breysse, Nondestructive evaluation of concrete strength: An historical review and a new perspective by combining ndt methods, Construction and Building Materials 33 (2012) 139–163.

[22] J. A. Hossack, P. Mauchamp, L. Ratsimandresey, A high bandwidth transducer optimized for harmonic imaging, in: 2000 IEEE Ultrasonics Symposium. Proceedings. An International Symposium (Cat. No. 00CH37121), Vol. 2, IEEE, 2000, pp. 1021–1024.

[23] A. Novak, M. Bentahar, V. Tournat, R. El Guerjouma, L. Simon, Nonlinear acoustic characterization of micro-damaged materials through higher harmonic resonance analysis, Ndt & E International 45 (1) (2012) 1–8.

[24] E. Barlow, A. J. Mulholland, A. Gachagan, A. Nordon, A theoretical investigation of chirp insonification of ultrasound contrast agents, Ultrasonics 51 (6) (2011) 725–733.

[25] S. Ménigot, J.-M. Girault, I. Voicu, A. Novell, Optimization of contrast-to-tissue ratio by frequency adaptation in pulse inversion imaging, IEEE transactions on ultrasonics, ferroelectrics, and frequency control 59 (11) (2012) 2431–2438.

[26] S. Ménigot, J.-M. Girault, Optimization of contrast resolution by genetic algorithm in ultrasound tissue harmonic imaging, Ultrasonics 71 (2016) 231–244.

[27] N. Houhat, S. Ménigot, T. Boutkedjirt, R. Drai, J.-M. Girault, Optimal stochastic excitation for linear flaw detection in a solid material, Lecture Notes in Computer Science 11401 (2019) 229–236.

[28] N. Houhat, V. Tournat, S. Ménigot, T. Boutkedjirt, J.-M. Girault, Optimal pump excitation frequency for improvement of damage detection by nonlinear vibro acoustic modulation method in a multiple scattering sample, Applied Acoustics 155 (2019) 222–231.

[29] K. H. Matlack, J.-Y. Kim, L. J. Jacobs, J. Qu, Review of second harmonic generation measurement techniques for material state determination in metals, Journal of Nondestructive Evaluation 34 (1) (2015) 273.

[30] A. Aseem, C. T. Ng, Debonding detection in rebar-reinforced concrete structures using second harmonic generation of longitudinal guided wave, NDT & E International 122 (2021) 102496.

[31] V. Gatsa, S. Ménigot, V. Tournat, Excitation frequency optimisation to enhance harmonics backscattered by a nonlinear medium, in: Forum Acusticum 2020, 2020, pp. 31–35.

[32] M. Ghrib, M. Rébillat, G. V. Des Roches, N. Mechbal, Automatic damage type classification and severity quantification using signal based and nonlinear model based damage sensitive features, Journal of Process Control (2018).

[33] D. Clements, J. Crawford, D. Joslin, G. Nemhauser, M. Puttlitz, M. Savelsbergh, Heuristic optimization: A hybrid ai/or approach, in: Workshop on Industrial Constraint-Directed Scheduling, 1997.

[34] J. D. Kelly Jr, L. Davis, A hybrid genetic algorithm for classification., in: IJCAI, Vol. 91, 1991, pp. 645–650.

[35] P. Siarry, Metaheuristics, Springer, Cham, Switzerland, 2016.

[36] R. L. Haupt, S. Ellen Haupt, Practical genetic algorithms, Wiley Online Library, 2004.

[37] J. A. Nelder, R. Mead, A Simplex Method for Function Minimization, The Computer Journal 7 (4) (1965) 308–313.